J. Earth Syst. Sci. (2019) 128:126
https://doi.org/10.1007/s12040-019-1144-3

Use of genetic algorithm in reservoir characterisation from seismic data: A case study

Satya Prakash Maurya[1], Nagendra Pratap Singh[1,*] and Kumar Hemant Singh[2]

[1] *Department of Geophysics, Institute of Science, Banaras Hindu University, Varanasi 221 005, India.*
[2] *Department of Earth Sciences, Indian Institute of Technology, Bombay, Mumbai 400 076, India.*
**Corresponding author. e-mail: singhnpbhu@yahoo.co.in*

MS received 11 January 2018; revised 16 June 2018; accepted 1 December 2018; published online 8 May 2019

In the present paper, a seismic inversion based on genetic algorithm (GA) is performed to characterise the reservoir using seismic data only from the Blackfoot field, Alberta, Canada. The algorithm is first tested on synthetically generated data to optimise the GA parameters. The error analysis between the inverted and the expected results suggested that the performance of algorithm is exceptionally satisfactory. Thereafter, the inversion is performed for real seismic data from the Blackfoot field. The seismic data is first inverted for acoustic impedance section and then it is transformed into the velocity and density sections using the relation derived from the well-log data. The interpretation of the inverted/derived results depicts a low-amplitude anomaly zone between 1055 and 1065 ms time interval, which is characterised as a reservoir. The results demonstrate the efficacy and applicability of the GA in reservoir characterisation from the seismic data alone. This study is very helpful for the offshore projects where the information about well logs are missing.

Keywords. Genetic algorithm; seismic inversion; reservoir characterisation; acoustic impedance.

1. Introduction

In integrated exploration and reservoir studies, seismic reservoir characterisation plays an important role as it provides an optimal understanding of the internal structures and properties of the reservoir (Bachrach *et al.* 2014). Nowadays, the estimation of reservoir properties using geophysical techniques has become a key process in oil and gas industries for performing prospect evaluation, reservoir characterisation and geological modelling (Li and Zhang 2011). In exploration projects, unveiling of deeper reservoir has always been a challenging task; which is riskier as well as expensive with the use of conventional reservoir characterisation techniques. The integrated seismic inversion and reservoir characterisation have emerged as a solution to this problem because they provide invaluable information related to exploration and production processes. Therefore, the oil industries worldwide are using integrated seismic inversion and reservoir characterisation as a tool for exploration and production activities.

Seismic inversion is a process that extracts subsurface petrophysical models from seismic and well-log data. In the absence of well-log data, the subsurface models can also be estimated from the inversion of seismic data alone (Krebs 2009; Azevedo *et al.* 2013). In oil and gas industry, seismic inversion technique has been widely used to locate subsurface reservoir (Morozov 2009). The petrophysical parameters that can be estimated

from the seismic inversion are impedance (Z), P-wave velocity (V_P), S-wave velocity (V_S) and density (ρ). The Lamê parameters ($\lambda\rho$ and $\mu\rho$) that are sensitive towards fluid saturation in rocks can also be derived from inverted impedance models. The biggest challenges of seismic inversions are that there may be more than one possible solution to the same problem (Russell 1988). The uncertainty of non-uniqueness can be reduced by using additional information that generally comes from the well-log data. Seismic inversion can be performed by using local optimisation techniques such as least square methods, steepest descent methods, conjugate gradient methods, quasi-Newton methods, Newton methods, etc. and/or global optimisation techniques such as simulated annealing, branch and bound algorithms, Bayesian search (partition) algorithms, genetic algorithms (GAs), etc. There are many examples of application of GA-based inversion techniques for characterisation of reservoir with or without the use of well-log data (Sen *et al.* 1995; Romero *et al.* 2000; Romero and Carter 2001; Dorrington and Link 2004; Velez-Langs 2005; Moncayo *et al.* 2012; Aleardi 2015; Aleardi *et al.* 2016). The present study belongs to the later class of studies and strengthens the possibility of reservoir characterisation from seismic data alone in the absence of well-log data. There are many examples of reservoir characterisation using various optimisation techniques such as model-based inversion, coloured inversion, sparse spike inversion (SSI), band-limited inversion (BLI), etc. on post-stack seismic data along with the well-log data of the area (Ferguson and Stewart 1996; Margrave *et al.* 1998; Larsen *et al.* 1999; Pendrel *et al.* 1999; Pendrel 2001; Dufour *et al.* 2002; Pendrel and Dickson 2003; Downton 2005; Swisi and Morozov 2009; Sena *et al.* 2011; Zheng *et al.* 2013; Dueñas and Davis 2014; Maurya and Singh 2015, 2017) but in this work we have attempted to characterise the Blackfoot reservoir on the basis of post-stack seismic data only using GA-based seismic inversion techniques.

The primary aim of the study is to assess the performance of seismic inversion based on the GA, which uses seismic data only and then identification of prospective zones in the Blackfoot field, Alberta, Canada. This study is very helpful to offshore projects where well-log information is sometimes missing and hence difficult to identify the prospective zone. The analysis and representation of results are performed in Matlab programming language software.

2. The study area: Blackfoot field, Canada

The Blackfoot field is located in the southeast of Strathmore city, Alberta, Canada. Pan Canadian Petroleum and the Consortium for Research in Elastic-Wave Exploration Seismology carried out the seismic survey to acquire seismic reflection data in 1996 (Dufour *et al.* 2002). The data was recorded in two overlapping patches: the first patch targeted the clastic Glauconitic channel and the second was planned to study the reef-prone Beaverhill lake carbonates (Lawton 1996). The dataset contains 708 shots into a fixed recording spread of 690 channels (Margrave *et al.* 1998). The bandwidth of the data is 5–90 Hz for the vertical component and 5–50 Hz for the horizontal component. The present study uses the data from the first patch. The processing steps used for the vertical and horizontal component data are well described in Simin (1996). In this study, the conventional (vertical component) 2D seismic data alone is used for reservoir characterisation using post-stack seismic inversion technique based on GA in contrary to the conventional procedure of reservoir characterisation using pre-stack or post-stack seismic data and well-log data to ascertain its efficacy for the purpose. The well-log datasets from the area are only used for cross validation of the results obtained from inversion based on GA.

The Glauconitic formation is of the Lower Cretaceous age, which represents sediment-filled incised valley of the upper Manville Group (Miller *et al.* 1995). The Glauconitic member consists of shale and sands of lacustrine and channel origin. Within the channel, the sediments are subdivided into three units corresponding to three phases of valley incision with different quality of sand deposits. These three units are not known to be found everywhere in the area (Dufour *et al.* 2002). The reservoir in the Blackfoot field is producing from the Glauconitic sand of the Lower Cretaceous Glauconitic formation. The stratigraphic column of the Blackfoot area is discussed in Margrave *et al.* (1998). Figure 1(a) shows the location of Blackfoot fields, Alberta, Canada (highlighted by the red rectangle) and the structure of the Mississippian horizon and the locations of the wells are shown in figure 1(b). The grain size of the Glauconitic formation varies from fine to medium. In this field, the eroded Mississippian carbonates are covered with Lower Cretaceous sediments. These sediments are the detrital member of variable thickness, while above this detrital member there are sheet and

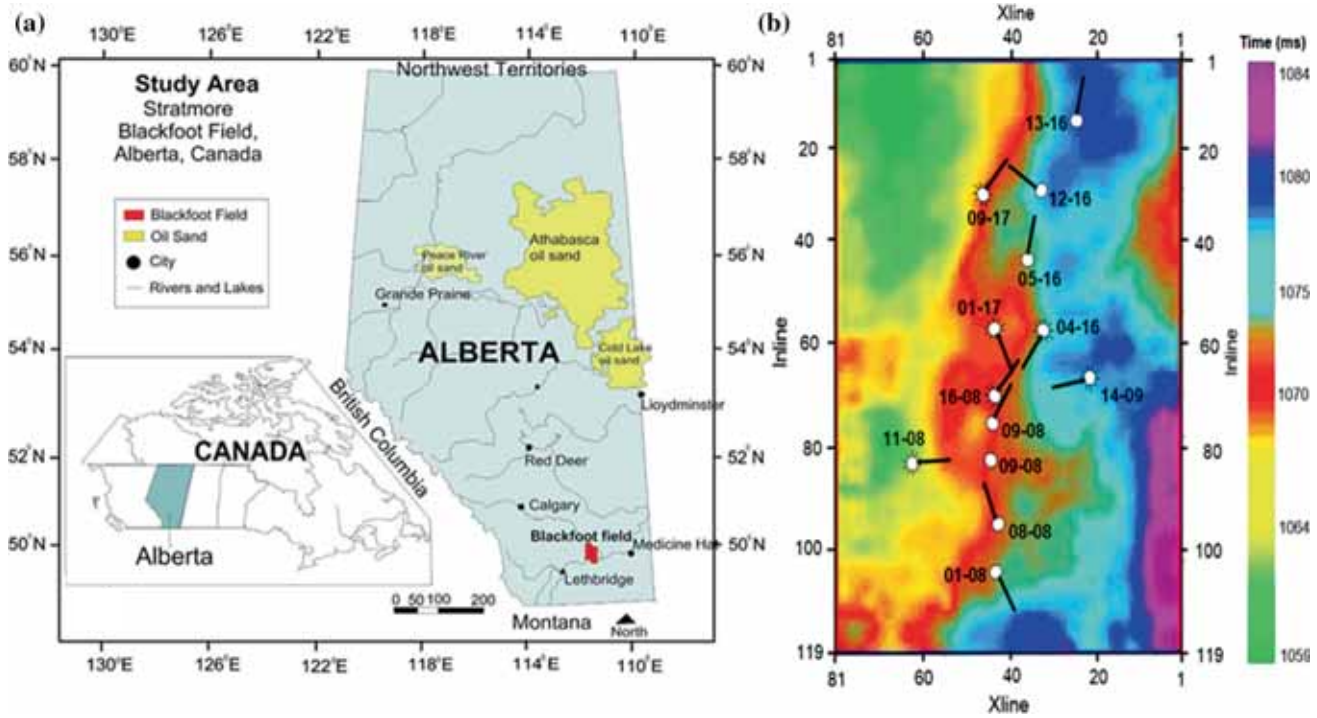

Figure 1. (**a**) Location of Blackfoot study area (red rectangle) and (**b**) structure of the Mississippian horizon and the locations of the wells.

ribbon Sunburst sands (Dufour *et al.* 2002). At a later time (Cretaceous), marine transgression deposited brackish shales, limestones and quartz sands and silts to build the Ostracod member.

3. Forward modelling

Forward seismic modelling is used for geological subsurface models of the Earth to simulate seismic field experiments. The model uses impedance series and generates synthetic seismograms (Connolly 1999). This synthetic seismogram is used for the testing of programs as the subsurface model is known (impedance model) and can be crosschecked with inverted/derived results. The synthetic seismogram is generated by convolution of wavelet with the Earth wavelets. The model parameter is acoustic impedance (AI) (Z) which is the product of velocity (V) and density (ρ):

$$Z = V\rho, \tag{1}$$

where Z is the AI, V is a p-wave velocity and ρ is the density. The reflectivity function can be calculated from the impedance as follows:

$$r_j = \frac{Z_{j+1} - Z_j}{Z_{j+1} + Z_j}, \tag{2}$$

where Z_j is the seismic impedance of jth layer and r_j is the seismic reflectivity of jth and $(j+1)$th interface. Thereafter, the synthetic seismogram is calculated from the reflection coefficient using the following equation:

$$S(t) = w(t) * r(t) + n, \tag{3}$$

where $S(t)$ is the synthetic seismogram, $w(t)$ is the source wavelet, $r(t)$ is the reflection coefficient of the subsurface and n is the additive noise and is generally assumed to be zero for simplicity.

4. Inversion using GA

GAs are global optimisation techniques, which use natural selection approach (Holland 1975). The algorithm is developed to find a geologically possible subsurface model of petrophysical characteristics (Bosch *et al.* 2010). The input is seismic data in time domain. The GA randomly generates impedance model (200 model) of the subsurface and then from this impedance series, synthetic traces are generated to examine the match between this synthetic trace with the corresponding seismic trace, if the error between them is small enough then the randomly selected impedance model is the solution, and if the error is not small enough,

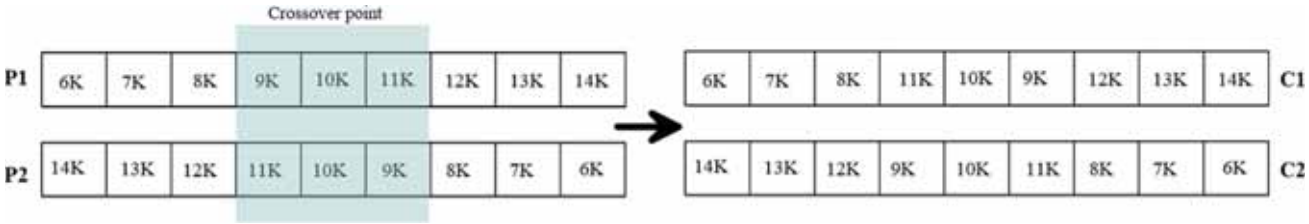

Figure 2. Process of two-point crossover. The highlighted zone depicts crossover point (K is 1000 multiple of a unit).

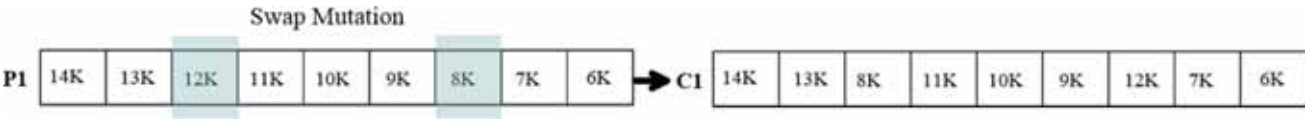

Figure 3. Process of mutation. The highlighted zone depicts the mutation points (K is 1000 multiple of a unit).

then the randomly generated impedance model is modified using GA parameters, i.e., Selection, Crossover and Mutation in a iterative way till the error gets small enough (Morgan *et al.* 2012). The detailed process used in this study is as follows.

The GA optimiser generates 200 random impedance solutions with uniformly distributed population under the limit 2250 to 21,000 m/s $\times$ g/cm^3. Thereafter, the first parameter of GAs, i.e., selection is used and two best solutions are selected on the basis of their fitness values. The process is as follows.

4.1 *Selection*

The synthetic trace is generated from random impedance model using the forward modelling procedure. Thereafter, the fitness values/error is estimated using the root mean square error formula between synthetic trace and corresponding real seismic trace as follows:

$$E = \frac{1}{n}\sqrt{\sum_{j=1}^{n}\left(T_{\mathrm{syn}j} - T_{\mathrm{real}j}\right)^2}, \qquad (4)$$

where E is the error, $T_{\mathrm{syn}j}$ is the synthetic seismogram and $T_{\mathrm{real}j}$ is the seismic trace and n is the number of observations (data points). On the basis of fitness values/errors, two best solutions (also called parents) are selected for further process (Hejazi *et al.* 2013). The next genetic operator is crossover, which modifies the selected solution with the hope of getting a better solution.

4.2 *Crossover*

Crossover helps in exchange of bits between two selected solutions (also called parents) to generate two new solutions (also called children). This process emulates the exchange of genetic traits during reproduction, where the child solutions inherit specific properties from both parents (Hejazi *et al.* 2013). Two-point crossover is used in the present study in the following way. Suppose the two best selected solutions are P1 and P2 (figure 2) and after two-point crossover, the new solutions (also called children) C1 and C2 are generated that would be better solutions of the problem compared with the parent solution (Hejazi *et al.* 2013). Figure 2 explains the two-point crossover process. The highlighted zone depicts the crossover points along which two-point crossover is performed. Thereafter, the next GAs parameter, i.e., Mutation is used to get better and better solution.

4.3 *Mutation*

Mutation increases the possibility of having a 'better-fit' solution better than those obtained after crossover. This purpose is fulfilled by randomly choosing and altering a bit (Padhi and Mallick 2013). Figure 3 shows the process of Mutation graphically. The highlighted zone depicts the mutation points along which the swap mutation is performed. After mutation, the final product is put back in the population to maintain population size and the same process is repeated until a termination criterion is reached.

4.4 *Termination criterion*

At this stage, the pool of solutions consists of a fixed percentage of original members and newly created offsprings. This pool is now considered as the next generation that can undergo Selection,

Crossover and Mutation all over again. This procedure is iterated until the misfit function reduces very close to zero or the pre-assigned number of iterations get over (Tran and Hiltunen 2012).

The inversion based on GA does not give absolute subsurface impedance model albeit it gives relative variation of AI. The practical process of GA is as follows.

(1) *Start:* generate random population within search space of n chromosomes (suitable initial guess solution for the problem).
(2) *Fitness:* estimate the fitness value $f(x)$ of each possible solution (chromosome).
(3) *New population:* generate new population by using the following steps:
   - Selection: select best two parent chromosomes from the population on the basis of their fitness value.
   - Crossover: do crossover between the parents to form a new offspring (children). If there is no crossover performed, the offspring will be an exact copy of parents.
   - Mutation: do mutation to mutate new offspring at each position.
   - Accepting: place this new offspring into the new population.
(4) *Replace:* Now use this new generated population for next iteration of the algorithm.
(5) *Test:* set end condition, and if the end condition is satisfied, stop the algorithm and return the best solution in current population.

Graphically, the methods are explained by a flow chart in figure 4.

5. Results

In this study, the inversion based on GA is applied in two steps. In the first step, the algorithm is tested over synthetically generated data for optimisation of parameters; and in the second step, it is applied to invert the real post-stack seismic data from the Blackfoot area and characterise the prospective zone without using well-log data.

5.1 *Algorithm testing*

For testing the algorithm, synthetic seismograms are generated and the algorithm is applied to estimate AI from these synthetic seismograms. A five-layer Earth's model is assumed with AI of 3600, 8800, 6000, 12,500 and 9200 $\mathrm{m/s\times g/cm^3}$. The result for a five-layer Earth's model is illustrated in figures 5 and 6. Figure 5 shows the synthetic example for five-layer Earth's model for noise free data, where figure 5(a) shows the synthetic seismogram, same trace shown eight times, figure 5(b) shows the five-layer Earth's model, figure 5(c) shows the Earth's reflectivity for five-layer model and figure 5(d) shows the comparison of inverted (black dot line) impedance and well-log impedance (red solid line).

The modelled AIs are compared with the inverted AIs. Figure 6(a) shows a collection of synthetic seismograms (same trace plotted eight times) for a quick comparison with addition of 5% random noises, whereas figure 6(b) shows the subsurface model. Figure 6(c) shows the reflection coefficients calculated on the basis of model AI. Figure 6(d) shows the comparison of model AI (solid red line)

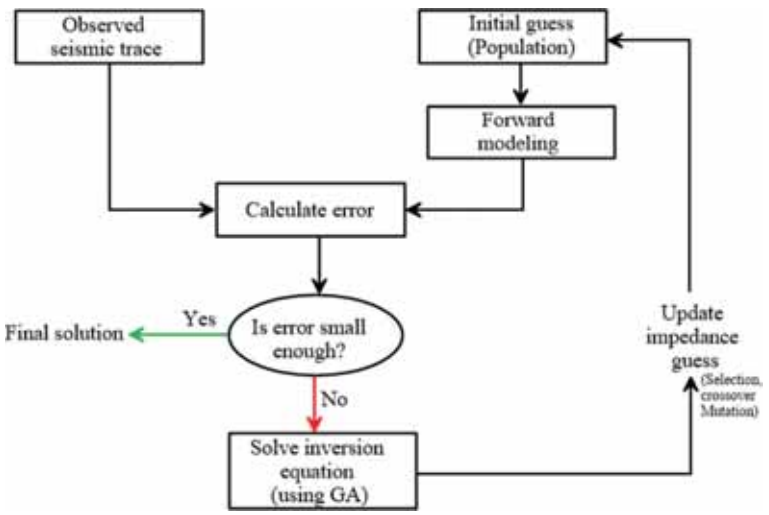

Figure 4. Flow chart of seismic inversion based on GA.

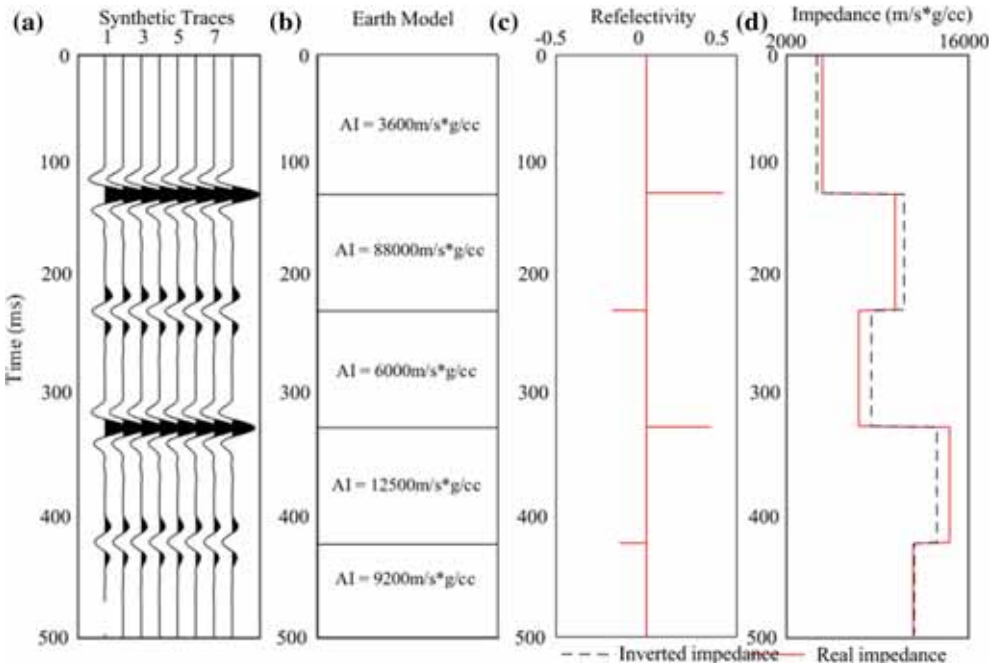

Figure 5. Synthetic example for a 5-layer Earth's model for noise free data where (**a**) synthetic seismogram, same trace shown eight times, (**b**) 5-layer of Earth's model, (**c**) Earth's reflectivity for a 5-layer model and (**d**) comparison of inverted (black dot line) and well-log impedance (red solid line).

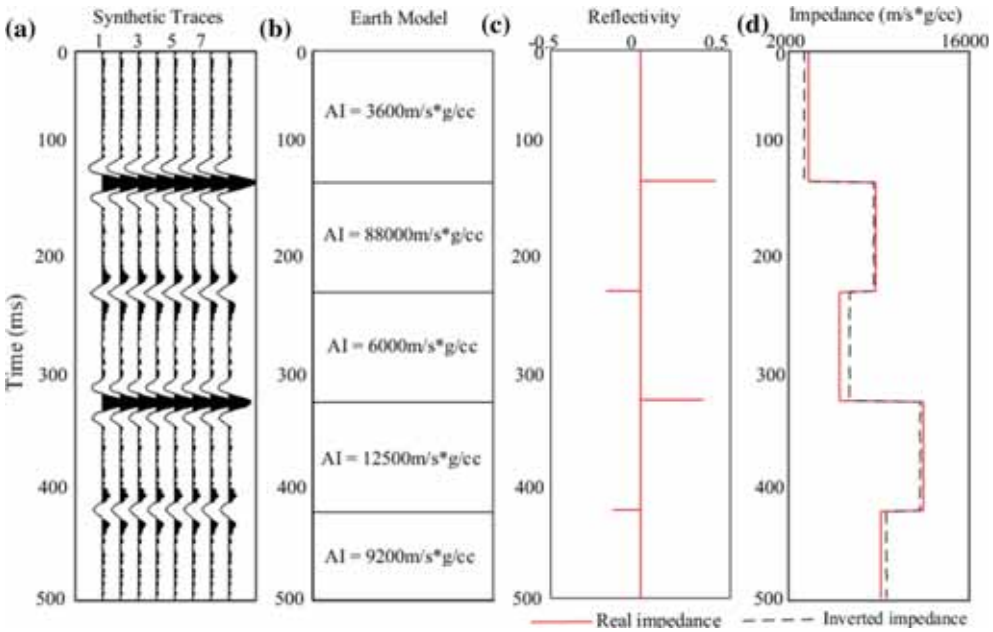

Figure 6. Synthetic example for a 5-layer Earth's model with 5% noise in the data, where (**a**) synthetic seismogram, same trace shown eight times, (**b**) subsurface model of AI, (**c**) estimated reflectivity, (**d**) comparison of modelled and inverted impedance.

and inverted AI (dashed black line). From figure 6, it can be examined that the inverted AI is very close to the modelled AI. The inverted AI shows small deviation with addition of noises in the data, however it follows the modelled AI trend very well.

Further, the numbers of layers are increased in the model and the inversion is performed for a 100-layer Earth's model. Figure 7 illustrates the inversion results for the 100-layer Earth's model. Figure 7(a) shows the synthetic trace generated using the forward modelling procedure and the

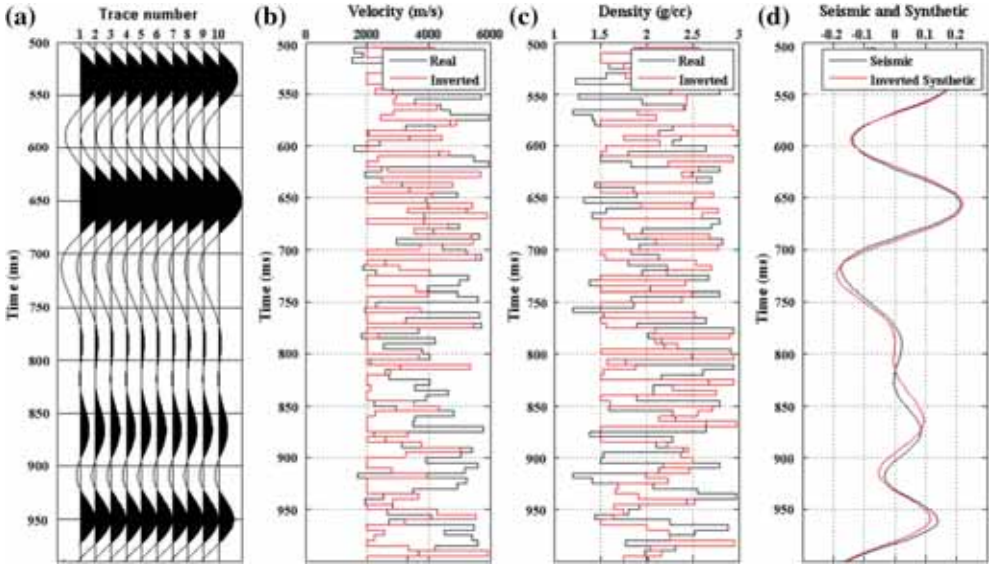

Figure 7. Synthetic example for a 100-layer Earth's model where (**a**) synthetic seismogram, same trace shown 10 times, (**b**) comparison of true velocity with the inverted velocity, (**c**) comparison of true and inverted densities and (**d**) seismic trace along with the inverted synthetic trace.

GA is applied to this synthetic trace to estimate AI and hence velocity and density combinations using the relationship between velocity and density with impedance from well-log data. Figure 7(b) shows the comparison of modelled velocity (black line) with the inverted/derived velocity (red line), whereas figure 7(c) shows the comparison of modelled density (black line) with inverted/derived density (red line). These velocity and densities are derived from AI using the relationship between the velocity and density with AI of the region. From results, it is noticed that the inverted/derived velocity and densities are in good agreement with the modelled velocity and density values, respectively. Figure 7(d) shows the comparison of modelled synthetic seismogram with the inverted synthetic seismogram and shows good agreement with each other. In both the cases (5-layer and 100-layer Earth's models), it can be observed that the inverted results are matching well with the original model values. The only difference observed is that when less number of layers is taken into the account, the inverted model matches more accurately with the real model when compared with the case when large numbers of layers are taken into the account. The one reason is that the inverted curves are not exact matches at the peaks and troughs and if large numbers of layers are present than it contains more peaks and troughs and hence shows small deviation. The other reason is that when sudden very high and low impedances are present in the data, the inversion is not exactly estimating it. The corresponding average correlation coefficients for the velocity and density are found to be 0.96 and 0.92 for 5-layer Earth's models and 0.91 and 0.93 for 100-layer Earth's models, respectively. This is obvious because with an increase in the number of layers the seismic trace generated over the model will have more number of peaks and troughs and as the inversion results do not exactly match at the peaks and troughs, and as a consequence of which the inverted results would deviate more and more from the real one with the increase in number of layers. Figure 8 shows the crossplot of real velocity and density with inverted velocity and density values. Figure 8(a) shows the crossplot of real and inverted velocity values, whereas figure 8(b) shows the crossplot of real and inverted density values for 100-layer Earth's model between time intervals of 800 and 1000 ms with non-uninform sampling interval. The red solid line is the best fit curve. It can be noticed from figure 8 that the scatter points are very close to the best fit line for both the cases (velocity and density) and depict good performance of the algorithm. After getting satisfactory results from the synthetic models, the algorithm is applied to the real seismic data to find the prospective zone.

5.2 *Application of GA to real data*

GA has been applied to the real post-stack seismic data from the Blackfoot field, Alberta, Canada. Only the post-stack seismic data (inline 65 and

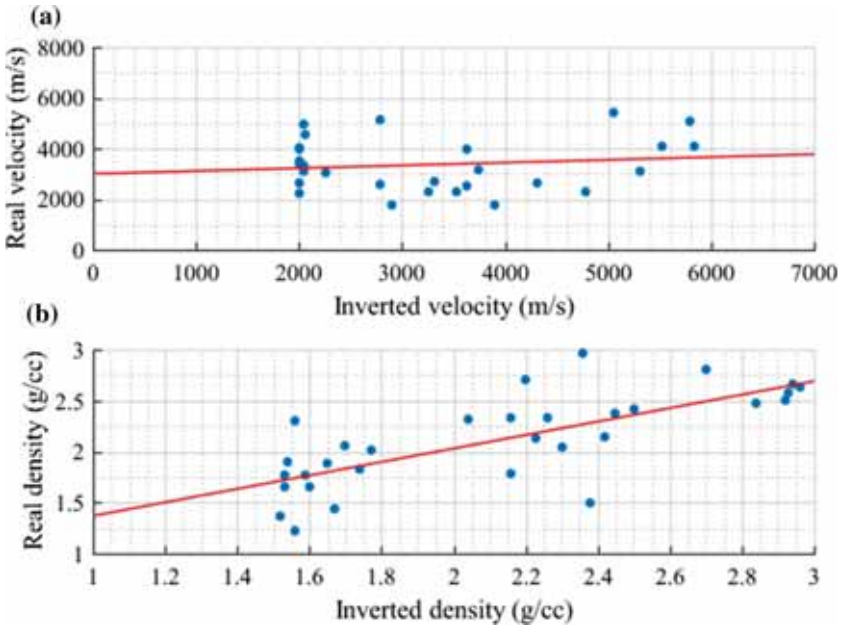

Figure 8. Crossplot of (**a**) real velocity *vs.* inverted velocity and (**b**) real density *vs.* inverted density for a 100-layer Earth's model. The red solid lines show the best-fit curve.

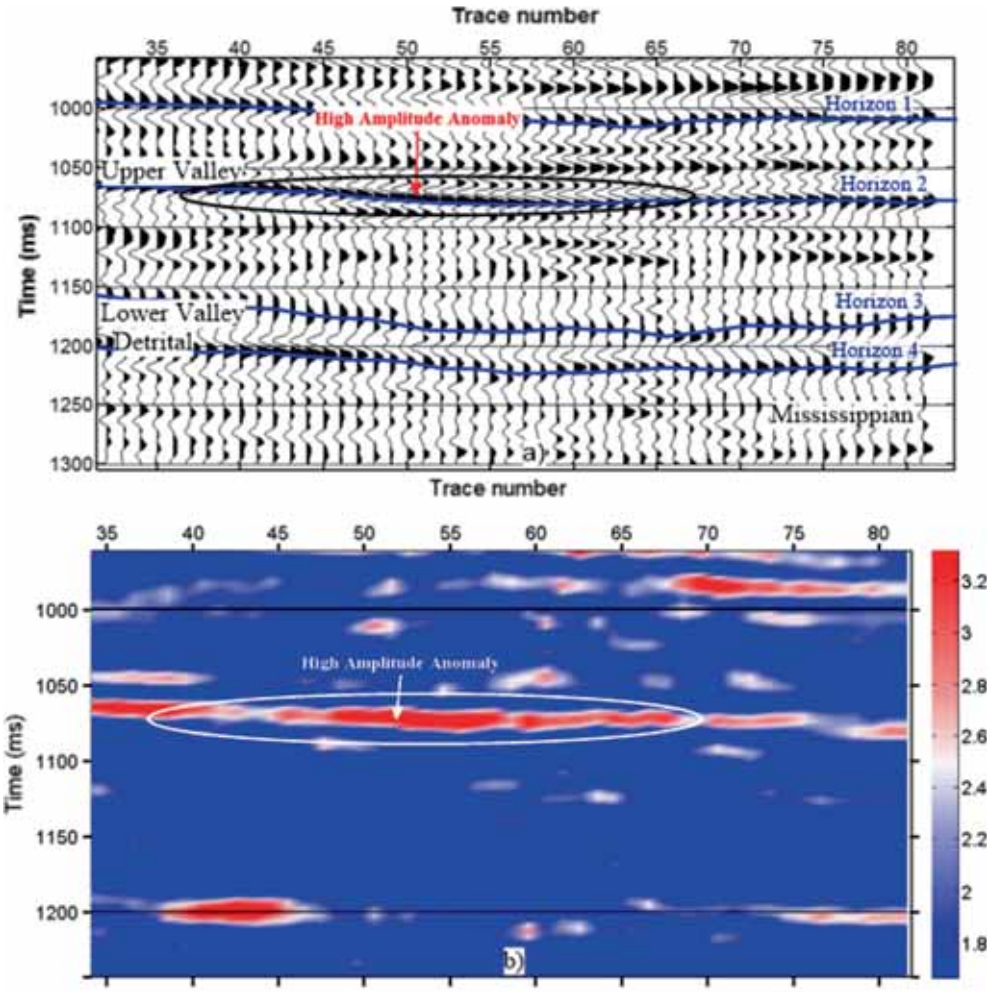

Figure 9. (**a**) Seismic section highlighted high amplitude anomaly and (**b**) the amplitude envelope of the seismic section depicts high amplitude anomaly by the ellipse.

crosslines 1–81) is used to characterise the reservoir using seismic inversion techniques based on GA.

Figure 9(a) shows the seismic data (inline 65) from the Blackfoot field, Alberta, Canada, which is used as input for seismic inversion. The high amplitude anomaly is highlighted by an ellipse with four picked horizons in seismic section. Signal envelope of seismic data is taken and shown in figure 9(b). The high amplitude anomaly is highlighted more clearly in signal envelope section compared to the seismic amplitude section. This high amplitude anomaly corresponds to shale–sand interface. The zone of interest is between 1000 and 1200 ms two-way travel time and the optimisation techniques are applied in this zone.

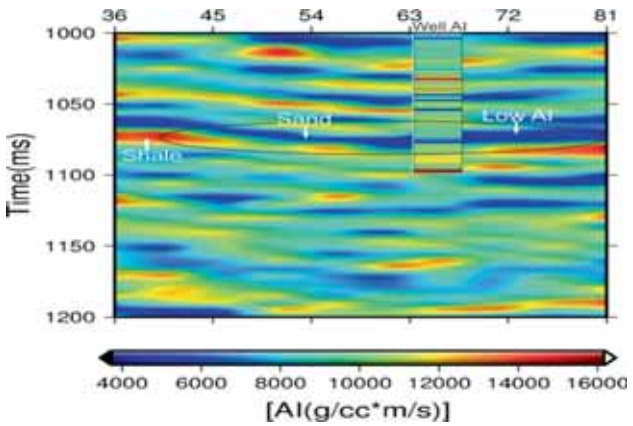

Figure 10. Cross-section of inverted AI at inline 65. The low-impedance zone is highlighted by the ellipse. The well-log AI is shown along a column at cross-line 65.

The algorithm is applied one by one to all seismic traces within the zone of interest (1000–1200 ms) and inverted for AI. Figure 10 shows the cross-section of inverted AI at inline 65. The analysis of the inverted AI section depicts an anomaly zone (low AI) between 1055 and 1065 ms TWT. This anomaly is well collaborated with high amplitude anomaly in seismic and amplitude envelope sections. The AI from well 01–17 is also plotted above the inverted AI section to see matching between them. Figure 10 shows that the inverted AI and well-log AI are matching well and describes the good performance of the algorithm. The AI anomaly can also be seen from well-log data at same location. To cross-check the inverted results, the inverted AI trace is cross-plotted with the near well-log AIs and shown in figure 11. Figure 11(a) shows the crossplot for well 01–17, whereas figure 11(b) shows the crossplot for well 08–08. The distribution of scatter points from the best-fit line depicts that the inverted results are in good agreement with the actual impedance.

Thereafter, the relationship between velocity and density with AIs is derived from well-log data, which is used to derive the velocity and density sections from the AI sections. According to Russell (1988), the velocity and density sections can be generated from AI section using the relationship derived from the well-log data but it provides mainly the qualitative interpretation. These derived velocity and density sections give average variation of the subsurface and cannot be relied

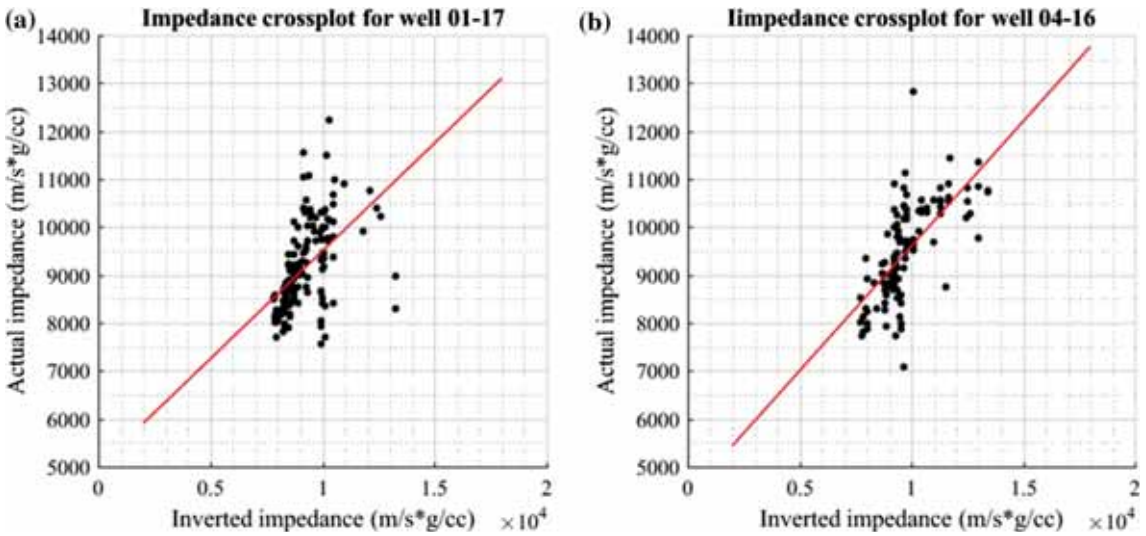

Figure 11. Crossplot of actual impedance and inverted impedance for (**a**) well 01–17 and (**b**) well 04–16. The red solid line indicates the best-fit line.

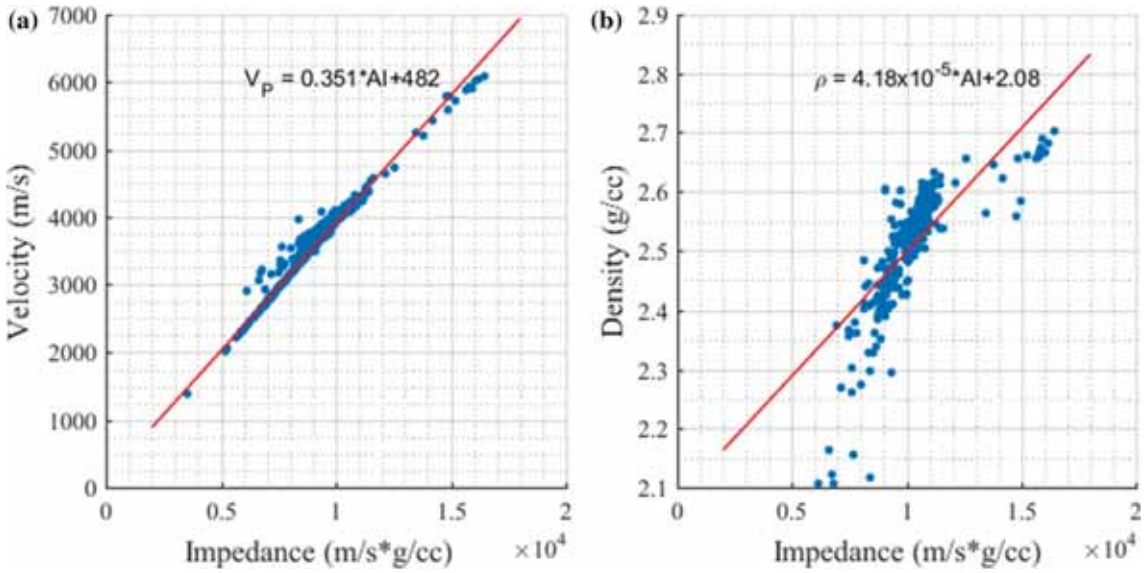

Figure 12. Crossplot of (**a**) velocity *vs.* impedance and (**b**) density *vs.* impedance for well 08–08. The best-fit line gives the relationship between velocity and density with AI.

on quantitative interpretation. Figure 12(a and b) shows the crossplot of velocity and density with AI for well 08–08, respectively. The best-fit line gives the relationship between velocity with AI and density with AIs. These relationships are given as follows:

$$V_{\mathrm{P}} = 0.351 \times \mathrm{AI} + 482, \tag{5}$$

$$\rho = 4.18 \times 10^{-5} \times \mathrm{AI} + 2.08. \tag{6}$$

Figure 13(a and b) shows the derived velocity and density sections generated using equations (5 and 6), respectively. Velocity and density from well-log data (01–17) are also plotted above the derived velocity and density sections to see the difference between the inverted and well-log values. It is noticed from figure 13 that the inverted velocity and density sections are matching with the well-log velocity and density values, respectively, quite well. The analysis of the derived velocity and density section shows anomaly between 1055 and 1065 ms time interval, which corroborates well with low AI and high amplitude anomaly and confirms the presence of the reservoir. The reservoir zone is characterised by low-velocity, low-density, low AI and high amplitude contrast values. The minimum RMS error is found to be 0.12 with a mean value of 0.20 during the optimisation. It is observed that the error decreases exponentially with an increase in the number of iterations (figure 14). The correlation coefficient between the inverted synthetic and real seismic is estimated to be 0.89. The

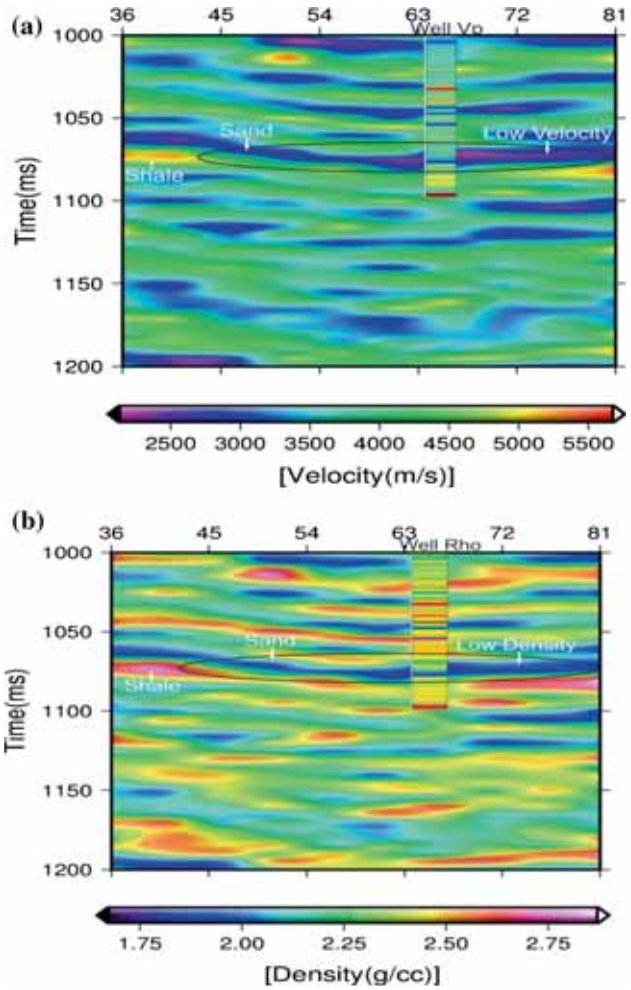

Figure 13. Cross-section of derived (**a**) velocity and (**b**) density sections at inline 65. The well-log velocity and density are plotted along a column at cross-line 65. The anomaly zone is highlighted by ellipse.

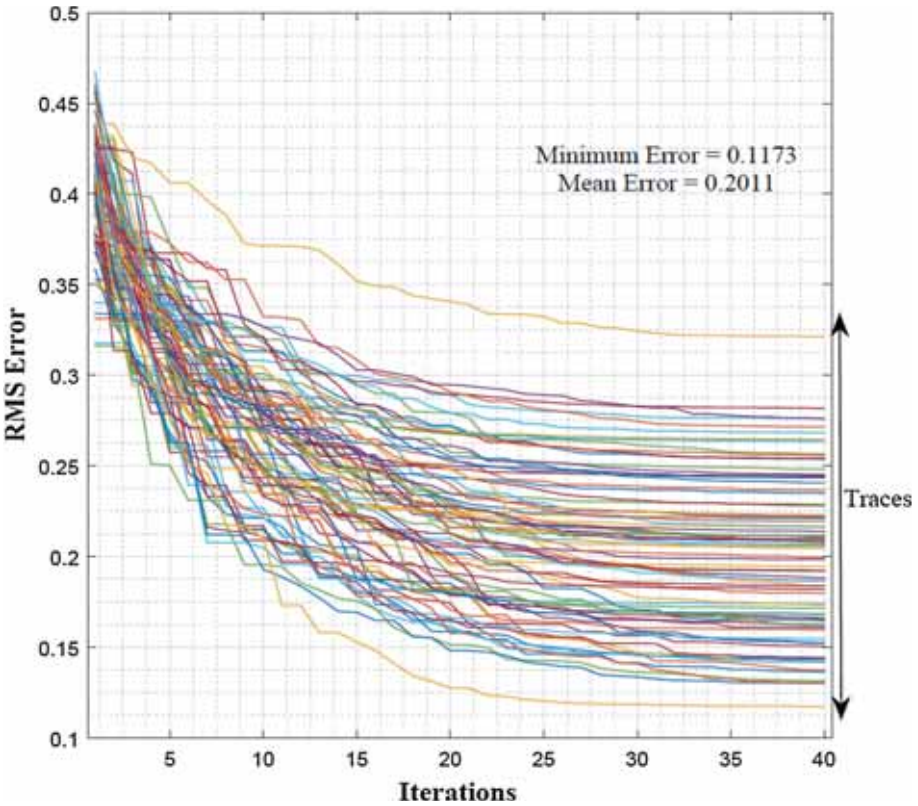

Figure 14. Variation of RMS error with iteration for all the seismic traces for inline 65.

Table 1. *Statistical analyses of genetic algorithm run for real seismic data.*

Properties	Velocity (m/s)	Density (g/cm^3)	Acoustic impedance ($m/s \times g/cm^3$)
Maximum	5998.8	3.00	17,984.4
Minimum	1500.0	1.50	2250.0
Standard deviation	1338.6	2.27	4664.9
Mean	3738.6	0.44	9031.0
Median	3734.1	2.27	8446.0
Mode	1501.0	1.50	2250.0
Range	4498.8	1.50	15,730.0
Correlation coefficient	0.87	0.89	0.8

maximum, minimum, standard deviation, mean, median, mode and range statistical analyses for real data are given in table 1. This analysis is performed on a single 2D line, but the results may vary for another inline acquired on the same channel.

6. Discussion

Seismic inversion techniques have been regularly used for analysing the seismic data to locate the reservoir zone. In this study, the aim of the inversion is to locate the reservoir zone that is clastic Glauconitic sand channel from the Blackfoot seismic data without using the well-log data. Since the sand reservoir is thin (∼35 m), it is hard to see the corresponding reservoir horizon in the seismic sections. First, seismic data is inverted for AI and then it is transformed into the velocity and density sections using the relationship derived from the well-log data. The analysis of results shows a reservoir zone between 1055 and 1065 ms time interval. Generally, the seismic and well-log data together are used to characterise the reservoir, but in this study we tried to locate the reservoir in seismic section without using well-log data and have successfully characterised the reservoir. For the cross validation of inverted/derived results, a comparison has been made with other inversion results,

i.e., with the band-limited impedance inversion (BLI) results (Maurya and Singh 2017) and SSI results (Maurya and Singh 2015) for the same area. Comparing the inversion results based on the GA with other inversion algorithms, it is concluded that:

(1) GA showed somewhat lower average impedance values in the reservoir zone compared to the other methods (sparse spike and band limited) and hence the AI contrast is more with the surroundings;
(2) GA appeared to give lower vertical resolution and decreases the horizontal layer consistency in terms of geology;
(3) no well-log information is needed for the inversion based on GA as the method randomly searches for possible solutions.

Figure 15 shows the graphical comparison of three post-stack inversion methods. Figure 15(a) shows the inverted impedance from linear programming sparse spike inversion (LPSSI) methods (Maurya and Singh 2015). For simplicity, the cross-section of inverted impedance is shown between 1000 and 1100 ms time intervals, which contains the reservoir zone. Figure 15(b–d) shows the inverted AI section derived using maximum likelihood sparse spike inversion (MLSSI) (Maurya and Singh 2015), BLI (Maurya and Singh 2017) and inversion based on GA techniques, respectively. In all the sections, the low impedance zone is highlighted by the rectangle between 1055 and 1065 ms time interval. The only difference is that the interpreted sand channel in SSI and BLI cases is between 1060 and 1065 ms time intervals, whereas it is 1055 and 1065 ms in the case of inversion based on GA. The boundaries are less clearly demarcated in the case of GA-based inversion in contrary to the case of SSI and BLI, where boundaries are more clearly defined.

Figure 16(a–d) shows the inverted/derived density section estimated using LPSSI (Maurya and Singh 2015), MLSSI (Maurya and Singh 2015), BLI (Maurya and Singh 2017) and inversion based on GA, respectively. A very low-density zone is highlighted in inverted density sections by the rectangle which is interpreted as a reservoir zone between 1060 and 1065 ms time interval for SSI and BLI cases and 1055 and 1065 ms for GAs case. These comparisons show that the inverted/derived impedance, density and velocities are the real subsurface models which are derived from post-stack seismic data only without using other information like well-log data. Although in some areas the resolution is poorer in inverted/derived results by using GA compared to the other popular methods but it searches successfully the prospective zone in a similar way. A quantitative comparison has been made particularly in the reservoir zone among the

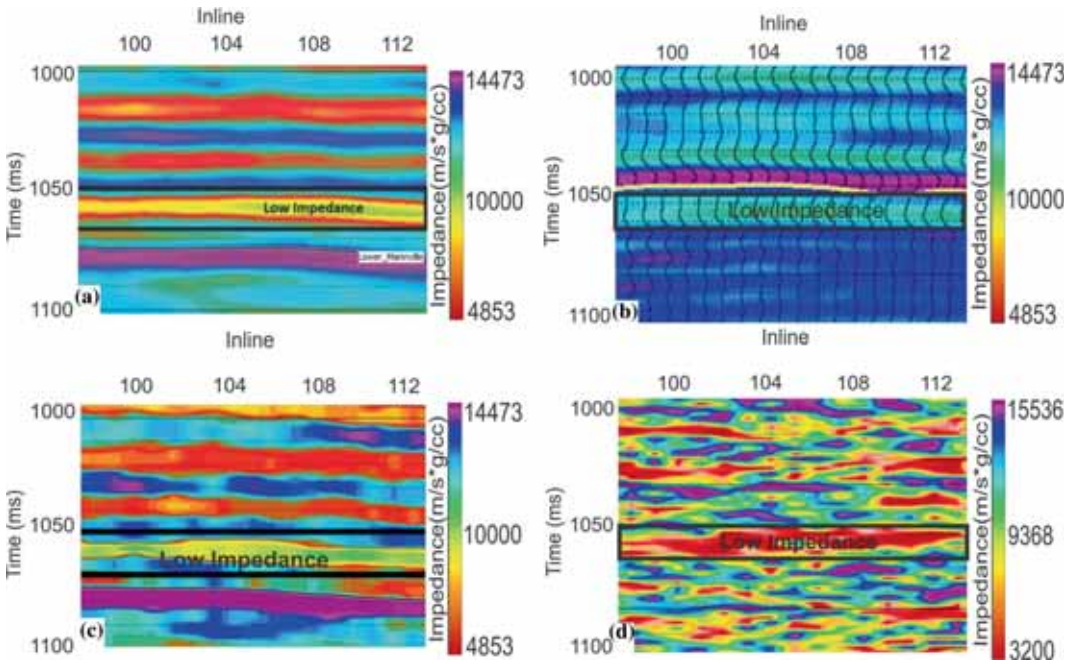

Figure 15. Cross-section of inverted AI at inline 65 estimated using (**a**) LPSSI (after Maurya and Singh 2015), (**b**) BLI (after Maurya and Singh 2017), (**c**) MLSSI (after Maurya and Singh 2015) and (**d**) inversion based on GA. All the sections show anomaly zone between 1055 and 1070 ms time interval.

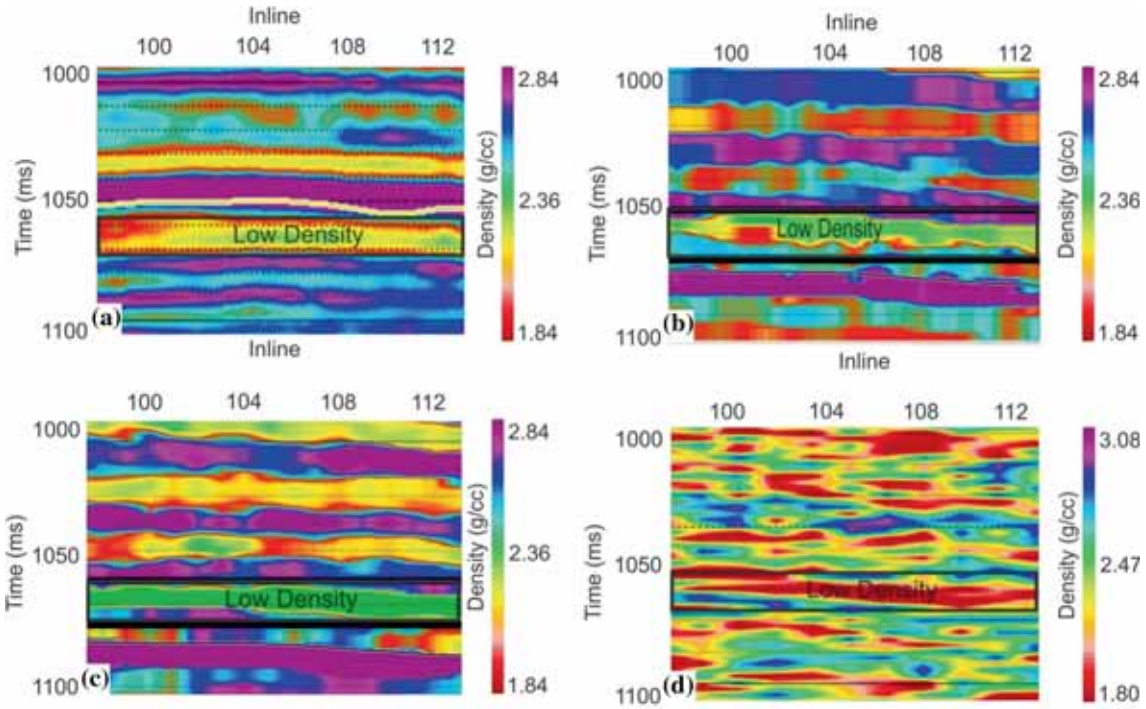

Figure 16. Cross-section of derived density at inline 65 estimated using (**a**) LPSSI (after Maurya and Singh 2015), (**b**) BLI (after Maurya and Singh 2017), (**c**) MLSSI (after Maurya and Singh 2015) and (**d**) inversion based on GA. All the sections show anomaly zone between 1055 and 1070 ms time interval.

Table 2. *Comparison of linear programing, maximum likelihood sparse spike, band-limited impedance inversion and inversion based on GA techniques in the reservoir zone (after Maurya and Singh 2015, 2017).*

	Sparse spike inversion			
Properties	LP	ML	Band limited	Genetic algorithm
Impedance (g/cm^3 × m/s)	6000–6600	7900–8200	7000–8000	3700–6000
Density (g/cm^3)	1.88–2.02	1.94–2.04	1.94–2.08	1.8–2.0
Correlation coefficient	0.97	0.95	0.89	0.89

SSI, BLI and inversion based on GA and is shown in table 2. This study is very much helpful for the offshore project where the well-log information is missing and cannot be derived using conventional inversion techniques, which use the well-log information for their implementation.

7. Conclusions

The present paper describes the application of GA on post-stack seismic data to demonstrate its efficacy and capability for reservoir characterisation using GA-based post-stack seismic inversion without using the well-log information. The performance is good for synthetic seismograms as well as for the real data. Although the correlation is lower for the real data compared to the synthetic data, the algorithm proved to be a very useful tool for obtaining information about subsurface features in the absence of well-log information. The use of GA provided high-resolution images of velocity, density and impedance models despite having very little a priori domain knowledge.

The inversion results of its application on real field post-stack seismic data indicated the presence of reservoir between 1055 and 1065 ms time interval, which validated well with the other inversion results from the same area. The algorithm showed the average correlation coefficients of 0.94 between generated and modelled synthetic data and 0.89 for the real data and inverted data which is reasonable considering the noise in the seismic trace and non-uniqueness inherent in an

inversion process. From this study, it is evident that GA can be successfully used for searching optimal solution and hence reservoir characterisation using the post-stack seismic data alone. Finally, it is concluded that the developed algorithm is very useful and suitable in search of new prospects such as in offshore exploration projects where no information about wells is available.

Acknowledgements

The authors are indebted to the Science and Engineering Research Board, Department of Science and Technology, New Delhi, for financial support and help in the form of National Postdoctoral Fellowship(NPDF) (Grant No.PDF/2016/000888). The authors would also like to acknowledge CGG Veritas for providing the seismic and well-log data from Blackfoot field, Alberta, Canada. The authors are also thankful to the anonymous reviewers whose suggestions have helped in improving the quality of the paper.

References

Aleardi M 2015 Seismic velocity estimation from well log data with genetic algorithms in comparison to neural networks and multilinear approaches; *J. Appl. Geophys.* **117** 13–22.

Aleardi M, Tognarelli A and Mazzotti A 2016 Characterisation of shallow marine sediments using high-resolution velocity analysis and genetic-algorithm-driven 1D elastic full-waveform inversion; *Near Surf. Geophys.* **14**(**5**) 449–460.

Azevedo L, Nunes R, Soares A and Neto G S 2013 Stochastic seismic AVO inversion; In: *75th EAGE conference and exhibition incorporating SPE, EUROPEC*, London, UK.

Bachrach R, Sayers C M, Dasgupta S and Silva J 2014 Seismic reservoir characterization for unconventional reservoirs using orthorhombic AVAZ attributes and stochastic rock physics modeling; *SEG Tech. Prog. Exp. Abstr.,* pp. 325–329.

Bosch M, Mukerji T and Gonzalez E F 2010 Seismic inversion for reservoir properties combining statistical rock physics and geostatistics: a review; *Geophysics* **75**(**5**) 75A165–75A176.

Connolly P 1999 Elastic impedance; *Lead. Edge* **18** 438–452.

Dorrington K P and Link C A 2004 Genetic-algorithm/neural-network approach to seismic attribute selection for well-log prediction; *Geophysics* **69**(**1**) 212–221.

Downton J E 2005 Seismic parameter estimation from AVO inversion; M.Sc. Thesis, Univ. of Calgary, Dept. of Geol. and Geophys., pp. 305–331.

Dueñas C and Davis T 2014 Reservoir characterization of the Montney Shale–integrating seismic inversion with microseismic; *First Break* **32**(**10**) 53–59.

Dufour J, Squires J, Goodway W N, Edmunds A and Shook I 2002 Integrated geological and geophysical interpretation case study, and lame rock parameter extractions using AVO analysis on the Blackfoot 3C-3D seismic data, southern Alberta, Canada; *Geophysics* **67**(**1**) 27–37.

Ferguson R J and Stewart R R 1996 Reservoir indication using V_p/V_s values derived from broad-band 3-C seismic data; *SEG Tech. Prog. Exp. Abstr.,* pp. 766–769.

Hejazi F, Toloue I, Jaafar M S and Noorzaei J 2013 Optimization of earthquake energy dissipation system by genetic algorithm; *Comput.-Aided. Civ. Inf.* **28**(**10**) 796–810.

Holland J H 1975 *Adaptation in natural and artificial systems*; The Univ. Michi. Press, Ann Arbor, MI, ISBN 10: 0472084607, ISBN 13: 9780472084609.

Krebs J R 2009 Fast full-wavefield seismic inversion using encoded sources; *Geophysics* **74**(**6**) WCC177–WCC188.

Larsen J A, Margrave G F and Lu H X 1999 AVO analysis by simultaneous PP and PS weighted stacking applied to 3C-3D seismic data; *SEG Tech. Prog. Exp. Abstr.,* pp. 721–724.

Lawton D S 1996 Design review of the Blackfoot 3C-3D seismic program; The CREWES Project Research Report, Vol. **8**, pp. 38-1–38-23.

Li X Y and Zhang Y G 2011 Seismic reservoir characterization: How can multicomponent data help?; *J. Geophys. Eng.* **8**(**2**) 123–141.

Margrave G F, Lawton D C and Stewart R R 1998 Interpreting channel sands with 3C-3D seismic data; *Lead. Edge* **17**(**4**) 509–513.

Maurya S P and Singh K H 2015 LP and ML sparse spike inversion for reservoir characterization: A case study from Blackfoot Area, Alberta, Canada; In: *77th EAGE conference exhibition*, Madrid, Spain.

Maurya S P and Singh K H 2017 Band-limited impedance inversion of Blackfoot field, Alberta, Canada; *J. Geophys.* **38**(**1**) 57–61.

Miller S L M, Harrison M P, Lawton D C, Stewart R R and Szata K J 1995 Analysis of P-P and P-SV seismic data from Lousana Alberta; CREWES Project Research Report, Vol. **7**, pp. 42-142–18.

Moncayo E, Tchegliakova N and Montes L 2012 Pre-stack seismic inversion based on a genetic algorithm: A case from the Llanos Basin (Colombia) in the absence of well information; *CT-F-Cienc. Tecn. Fut.* **4**(**5**) 5–20.

Morgan E C, Vanneste M, Lecomte I, Baise L G, Longva O and McAdoo B 2012 Estimation of free gas saturation from seismic reflection surveys by the genetic algorithm inversion of a P-wave attenuation model; *Geophysics* **77**(**4**) R175–R187.

Morozov I B 2009 Accurate post-stack acoustic-impedance inversion by well-log calibration; *Geophysics* **74**(**5**) R59–R67.

Padhi A and Mallick S 2013 Accurate estimation of density from the inversion of multicomponent pre-stack seismic waveform data using a non-dominated sorting genetic algorithm; *Lead. Edge* **32**(**1**) 94–98.

Pendrel J 2001 Seismic inversion: The best tool for reservoir characterization; *CSEG Recorder* **26**(**1**) 18–24.

Pendrel J and Dickson T 2003 Simultaneous AVO inversion to P impedance and V_p/V_s; In: *CSEG Ann. Meeting, Exp. Abstract.*

Pendrel J, Stewart R R, Dufour J, Goodway B and Van Riel P 1999 Offset inversion of the Blackfoot P-wave data and discrimination of sandstone and shales; In: *CSEG annual meeting, Expanded abstract*, pp. 289–300.

Romero C E and Carter J N 2001 Using genetic algorithms for reservoir characterization; *J. Petrol. Sci. Eng.* **31**(**2**) 113–123.

Romero C E, Carter J N, Gringarten A C and Zimmerman R W 2000 A modified genetic algorithm for reservoir characterization; In: *International oil and gas conference and exhibition in China*, Society of Petroleum Engineers.

Russell B 1988 Introduction to seismic inversion methods; *The SEG course notes series 2*.

Sen M K, Datta-Gupta A, Stoffa P L, Lake L W and Pope G A 1995 Stochastic reservoir modeling using simulated annealing and genetic algorithm; *SPE Formation Eval.* **10**(**01**) 49–56.

Sena A, Castillo G, Chesser K, Voisey S, Estrada J, Carcuz J, Carmona E and Hodgkins P 2011 Seismic reservoir characterization in resource shale plays: Stress analysis and sweet spot discrimination; *Lead. Edge* **30**(**7**) 758–764.

Simin V H 1996 Processing the Blackfoot 3C-3D seismic survey; CREWES Research Report, Vol. **8**, pp. 39-1–39-11.

Swisi A and Morozov I B 2009 Impedance inversion of Blackfoot 3D seismic dataset; In: *Proceedings of the CSPG CSEG CWLS conference, Expanded. abstract*, pp. 404–407.

Tran K T and Hiltunen D R 2012 One-dimensional inversion of full waveforms using a genetic algorithm; *J. Environ. Eng. Geophys.* **17**(**4**) 197–213.

Velez-Langs O 2005 Genetic algorithms in oil industry: An overview; *J. Petrol. Sci. Eng.* **47**(**1**) 15–22.

Zheng Y, Fang X, Fehler M C and Burns D R 2013 Seismic characterization of fractured reservoirs by focusing Gaussian beams; *Geophysics* **78**(**4**) A23–A28.

Corresponding editor: Arkoprovo Biswas